IOP Publishing | Astro Ltd Laser Physics Letters
Laser Phys. Lett. **19** (2022) 105207 (6pp) https://doi.org/10.1088/1612-202X/ac9062

Letter

Tailoring the pulse train of an optical frequency comb with a magnetized atomic medium

Yang Yan[1,2], Jinpeng Yuan[1,2,*], Lirong Wang[1,2,*], Liantuan Xiao[1,2] and Suotang Jia[1,2]

[1] State Key Laboratory of Quantum Optics and Quantum Optics Devices, Institute of Laser Spectroscopy, Shanxi University, 92 Wucheng Road, Taiyuan 030006, People's Republic of China
[2] Collaborative Innovation Center of Extreme Optics, Shanxi University, 92 Wucheng Road, Taiyuan 030006, People's Republic of China

E-mail: yjp@sxu.edu.cn and wlr@sxu.edu.cn

Received 15 August 2022
Accepted for publication 31 August 2022
Published 16 September 2022

Abstract

Selecting specific modes from the complete pulse train of optical frequency comb (OFC) is helpful in ultra-narrow linewidth laser preparation. Here, the mode selector for a commercial OFC based on the magnetized atomic medium is demonstrated in both theory and experiment. Only the comb modes with specific frequencies experience polarization rotation because of the Faraday effect, thus the mode tailoring can be realized by eliminating unchanged OFC modes via polarization selection. The theory study demonstrates the rich tunability of this device, and three specifically chosen operating conditions validate the system's characteristics. The selected pulse group is distinguished in both optical and frequency spectrum, where spectral differences and bandwidth can be observed accordingly. Further, the selected pulse group and a continuous-wavelength laser stimulate an electromagnetically induced transparency spectrum in the hyperfine Paschen–Back regime to show the pulse group characteristics in detail. The method proposed provides the experimental foundation for producing narrow linewidth lasers from a polychromatic source with tailored results retaining the excellent characteristics of the original.

Keywords: mode selection, optical frequency comb, electromagnetically induced transparency

(Some figures may appear in colour only in the online journal)

1. Introduction

The optical frequency comb (OFC) provides a highly periodic train of ultrashort pulses, representing remarkable stability with accuracy in time and frequency metrology, which can be employed in direct distance measurement [1, 2] and optical clock [3]. A single comb source can provide tens of thousands of optical frequency modes, which is beneficial for parallelization in wavelength division multiplexed systems [4, 5] as well as precise spectroscopy of atoms and molecules [6–9]. Meanwhile, extracting an individual pulse group while maintaining coherence and veracity is challenging but has urgent demands in arbitrary waveform generation and ultra-narrow linewidth laser preparation [10–13].

A commonly used method is the nested structure of optical cavities and Fabry–Perot etalons to select specific OFC modes that match their resonances [13–15]. Besides, sending a

* Authors to whom any correspondence should be addressed.

tunable laser into a long optical fiber to generate the stimulated Brillouin scattering signal is also employed as a method to extract a single OFC mode [12, 16]. Further, the optical phase-lock-loop is used to eliminate the noise of the optical signal and can be considered an efficient OFC filter [17]. Although the single frequency pulse can be selected from the OFC pulse train, prior arts can be improved in tunability. Therefore, more novel methods are always required to be introduced and researched.

The magnetic field can enhance the atomic medium's nonlinear dispersion, which alters the polarization direction of pulses with specific frequencies. Therefore, the magnetized atomic medium can become an advised mode selection device with premium tunability and efficiency via the precise polarization selection between the input and the output port. Recently, the magnetized atomic medium as the filter was widely studied when continuous-wavelength (CW) laser served as the source [18] and achieved excellent performance by geometry redesigning, wavelength division multiplexing, and cascaded vapor cells [19–21]. The medium has also been applied in quantum optics [22, 23] and frequency standards [24]. However, the powerful tools in frequency tailoring have not been applied to polychromatic sources, and many details still need to be considered.

In this work, a mode selector for a commercial OFC based on the magnetized atomic medium is realized in both theory and experiment. This device, provided by the Faraday rotation effect, shows abundant tunability around atomic transition frequency and is verified experimentally by different parameter combinations. Three typical selector profiles are chosen for specific atomic spectra [25], demonstrating flexibility to various demands [26, 27]. The output pulse groups from the selectors are inspected in both optical spectrum and heterodyne beat notes, and the nature of the mode selector is shown adequately. A selected pulse group is further studied and sent into the atoms under the magnetic field together with a CW laser to form the electromagnetically induced transparency (EIT) spectrum in a V-type energy level system. This proposed method paves the foundation for preparing a single pulse source from a polychromatic source, maintaining the outstanding features of the original.

2. Experiment setup

Figure 1 shows the experimental system, consisting of four parts: comb, mode selector, distinguish, and EIT. In the comb part, a fiber-based mode-locked OFC from Menlo systems (FC1500-250) generates a pulse train with the central offset frequency f_{ceo} of 20 MHz and the repetition frequency f_{rep} of 250 MHz. An SHG module is used for frequency doubling and converts the central wavelength from 1560 nm to 780 nm, which couples rubidium's typical transitions.

In the mode selector part, the combination of the half-wave plate (HWP1) and Glan-Taylor prism (GTP1), with an elimination ratio of $1{:}10^5$, ensures the incident pulse train with a high-purity horizontal linear polarization. Then the input pulse train polarization is varied by atoms' nonlinear dispersion under the influence of strong magnetic fields provided by magnetic field generators (MG1). GTP2, orthogonal to GTP1, filtrates the horizontal polarization components of pulses with high isolation. Therefore, the pulse train is tailored into a pulse group and then divided via a fiber-based 50:50 coupler, which will be sent to the following two parts.

The distinguish part firstly verifies the validity of the selector by feeding the tailored pulse groups into a high-resolution optical spectrum analyzer (OSA) (AQ6370C, Yokogawa). Then, a 780 nm CW laser from an external cavity diode laser (DL pro, Toptica) is adjusted by HWP2 to match the polarization direction of the pulse group. The laser frequency is locked to atomic transition via saturated absorption spectroscopy. The tested pulse group and CW laser intersect at the beam splitter, then completely overlap in space and interfere to produce beat notes, which are obtained by a high-speed optical receiver (1414, Newport) and analyzed in a spectrum analyzer (EXA signal analyzer, Keysight). In the EIT part, the selected pulse group and a 795 nm laser (DL pro, Toptica) are overlapped spatially and interact with atoms in a vapor cell. The vapor cell is filled with isotopically enriched ^{87}Rb and covered with an intense magnetic field. The pulse group as the probe is amplified by an avalanche photodiode with CW laser eliminated via a bandpass filter.

3. Theoretical analysis

When magnetic field is absent, the refractive index n of the atomic medium can be represented as:

$$n(T)^2 = 1 + \frac{N(T)\, e/m\varepsilon_0}{\omega_0^2 - \omega^2} \tag{1}$$

where N indicates the atom population, e and m are the charge and mass of the atom, respectively, ε_0 describes the permittivity of vacuum, ω_0 represents the natural transition angular frequency, and ω stands for the laser angular frequency.

The linear polarized laser can be considered coherent superimposed on the right-handed and left-handed circularly-polarized components. Under the Zeeman effect from the magnetic field strength B, the magnetic sublevels no longer degenerate. The transition frequencies corresponding to the right-handed and left-handed circularly polarized components are related to Larmor frequency $\omega_{\mathrm{L}} = \frac{e}{m}B$, and the specific transition frequencies can be expressed as $\omega_0 + \omega_{\mathrm{L}}$ and $\omega_0 - \omega_{\mathrm{L}}$. Correspondingly, the medium refractive indexes n_R and n_L are shown as $n_{\mathrm{R}}^2 = 1 + \frac{N(T)e/m\varepsilon_0}{(\omega_0+\omega_{\mathrm{L}})^2-\omega^2}, n_{\mathrm{L}}^2 = 1 + \frac{N(T)e/m\varepsilon_0}{(\omega_0-\omega_{\mathrm{L}})^2-\omega^2}$.

When the two components travel through the atomic vapor cell, a phase difference occurs while propagating for the same length $z = d$, which is reflected as the rotation of the polarization axis of the linear polarized laser in macroscopic. The rotation angle θ is described as $\theta = \frac{(n_{\mathrm{R}}-n_{\mathrm{L}})\omega d}{2c}$, where c represents the speed of light in vacuum [28]. There are few differences among n_{R}, n_{L} and n, so that we approximate that $n_{\mathrm{R}} - n_{\mathrm{L}} \approx \frac{n_{\mathrm{R}}^2 - n_{\mathrm{L}}^2}{2n}$. Also notice that $\omega_{\mathrm{L}}^2 \ll \omega^2$, so ω_{L} terms are ignored.

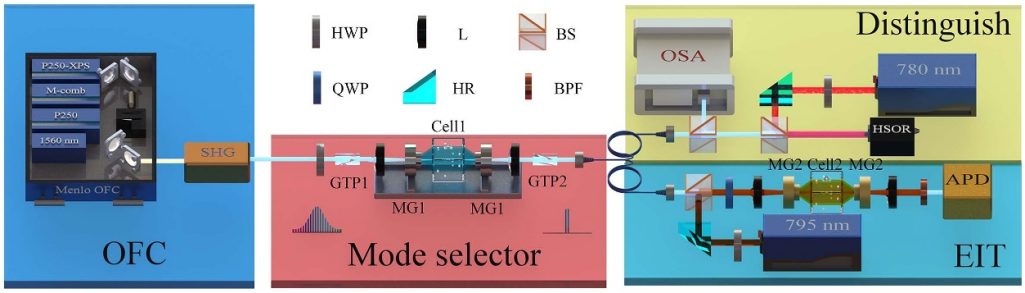

Figure 1. Experimental setup. SHG, second harmonic generator; HWP, half-wave plate; BS, beam splitter; L, lens; QWP, quarter-wave plate; HR, high reflectivity mirror; BPF, bandpass filter; GTP, Glan-Taylor prism; MG, magnetic field generator; Cell 1, vapor cell of Rb in natural abundance; Cell 2, vapor cell of isotopically enriched ^{87}Rb; OSA, optical spectrum analyzer; HSOR, high-speed optical receiver; APD, avalanche photodiode.

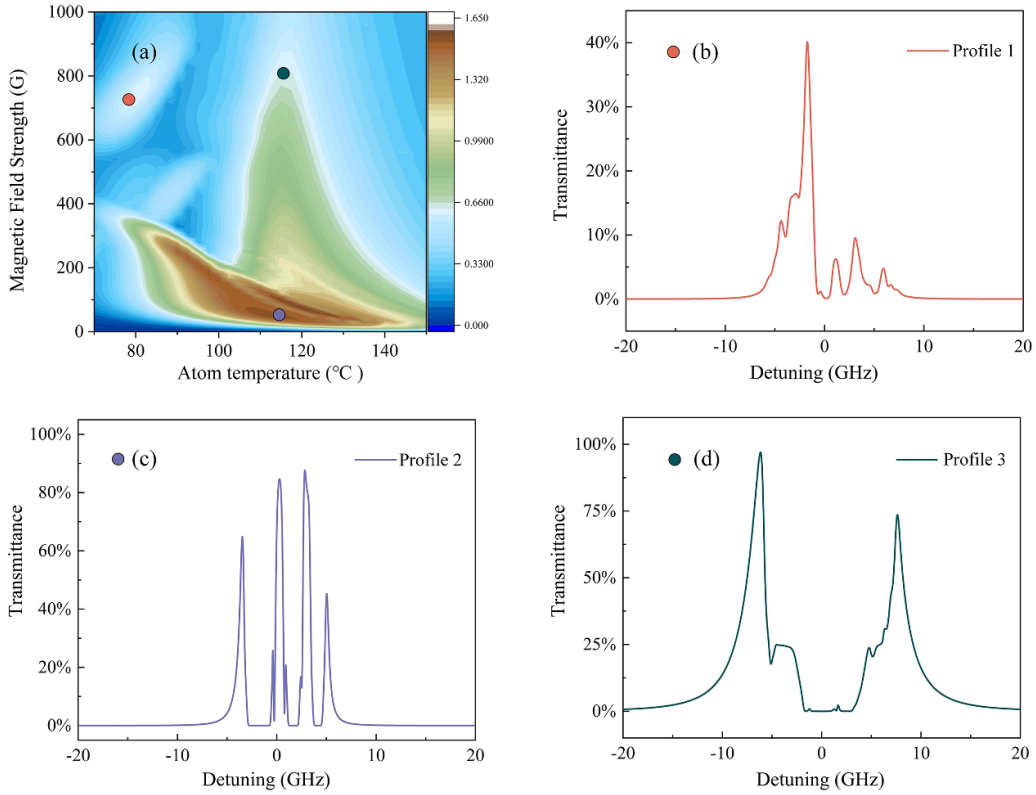

Figure 2. (a) Contour of X factor as a function of atom temperature and magnetic field strength. (b)–(d) Three typical profiles of the mode selector.

Therefore, the rotation angle θ that alters with magnetic field B is expressed as:

$$\theta = e\omega \frac{\mathrm{d}n(T)}{\mathrm{d}\omega} Bd \tag{2}$$

where $\frac{\mathrm{d}n(T)}{\mathrm{d}\omega}$ represents the dispersion of the medium. It can be seen that the Faraday rotation angle θ will be variable with varying the combinations of atom temperature T and magnetic field strength B. The transmittance of the mode selector depends on the proper polarization rotation.

The X factor is introduced when we have the freedom to select the exact operating condition for the desired OFC mode, which is given as following [29]:

$$X = \frac{Tr_{\max}}{\mathrm{BW} \times \mathrm{Num}} \tag{3}$$

where $Tr_{\max}$ is the maximum transmittance in the spectrum, BW represents the equivalent bandwidth of the selector, and Num stands for the number of OFC modes accommodated in the equivalent bandwidth. Here, $\mathrm{BW} = \frac{\int_0^\infty Tr(\nu)\mathrm{d}\nu}{T_{\max}}$ and $\mathrm{Num} = \frac{\mathrm{BW}}{D}$, ν is the laser detuning, and D is equal to the f_{rep} of OFC.

Equation (2) shows the performance of the mode selector, which depends on the atom temperature and magnetic field strength. Therefore, the relationship of the X factor as a function of the two parameters for naturally abundant rubidium is studied and plotted as shown in figure 2(a). The magnetic

field strength range is from 0 to 1000 G, and the atom temperature range is from 70 °C to 150 °C. The diverse parameter combinations shift the mode selector's performance and satisfy the requirements of applications. During the magnetic field strength below 500 G, there is a prominent peak for the *X* factor. In this area, only specific OFC modes can travel through the mode selector, thus the operating condition is conducive to selecting as few as possible or even a single OFC mode. With the atom temperature rising, the mode selector offers a high *X* factor as more atoms participate in the interaction. In contrast, the transmission range expands, and the transmittance reduces so that the *X* factor gradually decreases with the increment of magnetic field strength. The spectral split occurs, and bandwidth reduces because of the Zeeman effect. After the magnetic field strength exceeds 500 G, the bandwidth maintains high due to a sizable background transmittance, so the *X* factor is restrained. In this area, many OFC modes can traverse through the mode selector. Therefore, such an operating condition can provide a tailored pulse group with full-spectrum characteristics. The more detailed experimental results for the mode selectors can be seen in our previous work [20]. A mode selection system covering an optional range of 40 GHz is successfully built around the operating wavelength, which means 160 OFC modes are switchable.

Figures 2(b)–(d) show three typical profiles of mode selectors. Figure 2(b) shows profile 1 which has one prominent transmission peak and two side peaks, operating at 80 °C & 720 G. The central transmission peak shows high transmittance and narrow full width at half maximum (FWHM), while side peaks can be ignored for the poor power per OFC mode. For profile 2 in figure 2(c), the selector shows four transmission peaks of similar height, operating at 117.5 °C & 50 G. Each transmission peak can only get one or two OFC modes through, while multiple transmission peaks make full-spectrum characteristics maintained. In figure 2(d), profile 3 represents a standard twin transmission peak selector profile, operating at 117.5 °C & 760 G. The two prominent transmission peaks have wide FWHM and high transmittances, which can serve as a notch filter to eliminate the OFC mode between the two peaks.

4. Results and discussion

Figure 3 shows the optical spectra as the verification of three parameter combinations of profiles mentioned in figures 2(b)–(d). The OFC's direct optical spectrum is shown as the background. The spectral intensity differences among profiles come from the coherent accumulation of the amplitude of the selected pulses, and the differences in the tailored pulse groups' center frequencies appear as the FWHM of the spectra. Also, all three profiles bring narrow and high transmission peaks around 780 nm, but there are still tiny peaks at 795 nm, which is consistent with our previous work [20]. The direct detection in the optical spectrum shows the mode selector's high isolation in the wavelength magnitude. The adopted operating condition of the mode selector in the following verifications is the same as profile 1 in figure 2(b) because of its

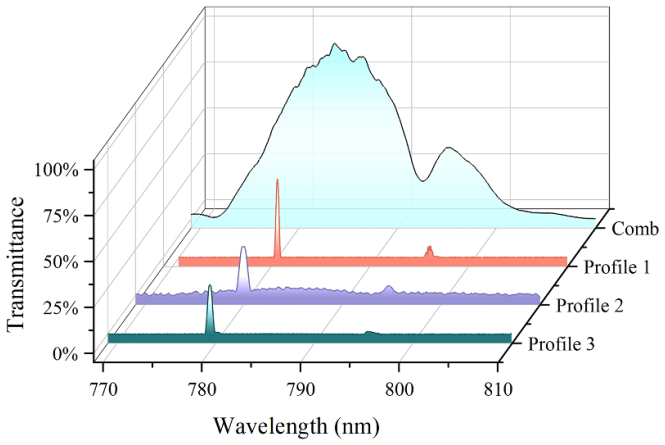

Figure 3. Optical spectra of OFC and selected pulse groups from OSA.

narrowest FWHM among the three operating conditions. In addition, further detection in the frequency domain needs to be carried out since the OSA's limited resolution of 0.02 nm.

Figure 4 shows the frequency spectrum of the beat notes among the CW laser and tailored pulse group. A schematic of pulses, CW laser, and beat notes is shown in the inset. A 780 nm CW laser, whose frequency is locked by saturated absorption spectrum, is used to interfere with the pulse group and get the pulses' exact frequency information through beat notes. The OFC mode nearest to the CW laser is set as the n_{th} mode, and other OFC modes are marked in turn. Every two lights (pulse or laser) with different frequencies generate a beat note, and the frequency of the beat note is equal to the frequency shift between two lights. The corresponding relationships are marked in the figure as α-ζ, showing the beat notes between f_i and f_j, where i and j represent OFC mode or CW laser. Note that the δ and ε peaks have the same color because they represent the beat note between the adjacent OFC modes and also appear as the same peak in the frequency spectrum.

After the introduction of the inset, the experimental frequency spectrum in figure 4 gets clear explanation. The resolution bandwidth is 100 kHz, and the video bandwidth is 1 kHz. Note that there are only three main CW-pulse beat notes, which proves the high efficiency and isolation of the mode selector around the target wavelength. The amplitudes of three CW-pulse beat note peaks show a declining tendency, owing to the increasing frequency differences and the inherent transmission variation of the mode selector. Besides, a series of peaks appear at $f = m \times 250$ MHz for the interference among adjacent OFC modes and constant repetition frequency of OFC, and m has a maximum value of 2 in this spectrum.

We use the tailored pulse group to perform atomic spectroscopy to further test the results of the tailored OFC in the frequency domain. In figure 5(a), an energy level schema of ^{87}Rb clearly expresses the mechanism of the displayed spectrum. A 795 nm CW laser serves as a pump laser and scans over the $5S_{1/2}-5P_{1/2}$ transition of rubidium. The three selected OFC modes work as probes, and the frequency intervals between two adjacent combs remain 250 MHz. Besides, by

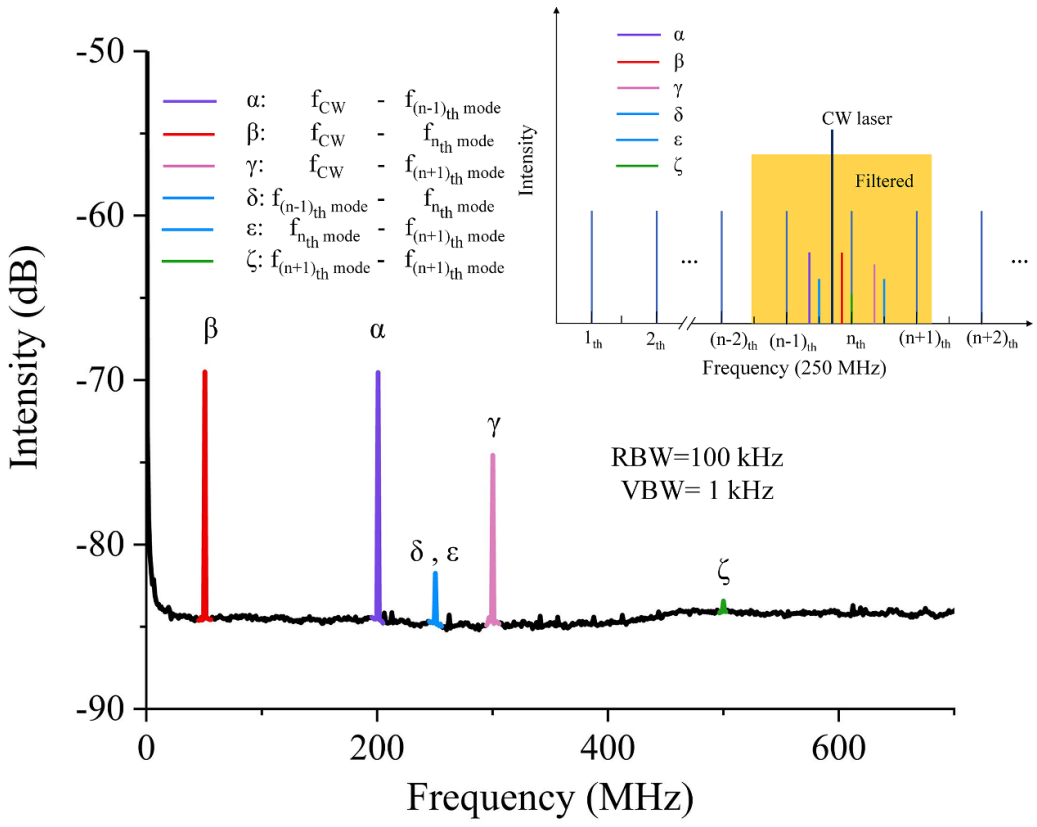

Figure 4. The experimental frequency spectrum of the beat notes among the tailored pulse group and CW laser. The inset is the schematic of pulses, CW laser, and beat notes. α-ζ, the beat notes between f_i and f_j, where i and j represent OFC mode or CW laser.

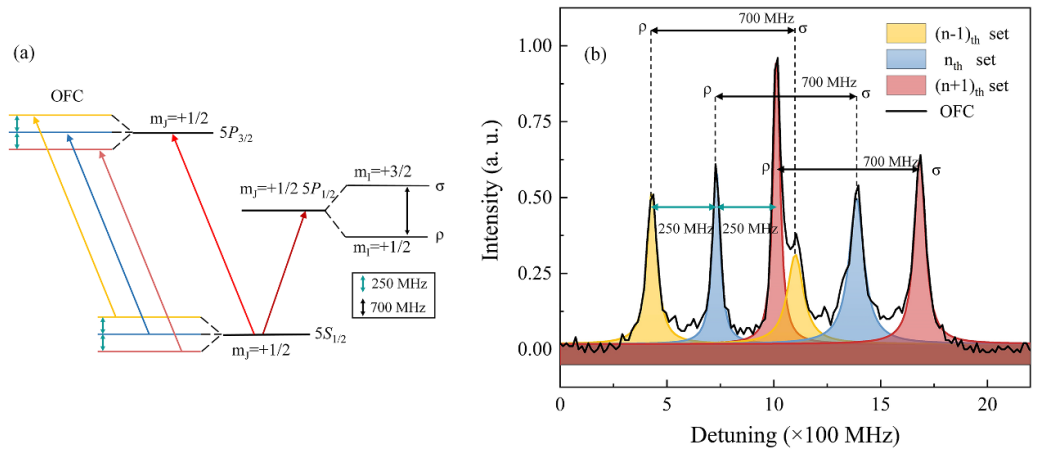

Figure 5. (a) Energy levels of ^{87}Rb EIT in V-type energy level system. (b) EIT spectrum generated from pulse group and CW laser.

applying an intense magnetic field, the magnetic sublevels no longer degenerate with the frequency shifts separated by more than the Doppler width. Apparent pulse features can be seen due to the hyperfine Paschen-Back effect. As a result, the frequency interval between two adjacent magnetic sublevels with different m_I values reaches 700 MHz under the magnetic field strength of 0.3 T [30], marked as σ and ρ.

Figure 5(b) shows three sets of EIT spectra. The vapor temperature is 50 °C, and the magnetic field strength is 0.3 T in cell 2. The $5S_{1/2}$ ($F = 2$)-$5P_{1/2}$ ($F = 2$) transition frequency of ^{87}Rb is the zero-detuning. Different colors (red, yellow, and blue) distinguish three sets of EIT spectra, each consisting of a pair of twin peaks. The frequency difference between twin peaks is 250 MHz, the same as the f_{rep} of the comb, and shifts among peak sets, 700 MHz, are consistent with the hyperfine Paschen-Back effect calculation results. The mode selector provides frequency-dependent intensity disparity for OFC modes, resulting in the power distinctions for each transmission peak. Compared with the traditional direct frequency comb spectrum, the atomic spectrum from the tailored pulse group is more transparent and intuitive, reducing the difficulties in distinguishing and calculating [31].

5. Conclusions

In this work, we realized a mode selector for a commercial OFC based on the magnetized atomic medium both theoretically and experimentally. Three selector profiles are chosen for specific atomic spectra, demonstrating adaptability to demands. The output pulse groups from the selectors are distinguished in both optical and frequency spectrum. Moreover, one of the extracted pulse groups is used to demonstrate an EIT spectrum with a V-type energy level system in a strong magnetic field, showing high transmittance and isolation of the selector. In contrast with the previous OFC mode selector, the proposed method ensures the mode selection ability and dramatically enhances the tunability while avoiding introducing the slave laser. This work expands the field of tailoring polychromatic source and pave waves for precision spectroscopy and ultra-narrow bandwidth laser preparation.

Acknowledgments

This work is supported by the National Natural Science Foundation of China (61875112, 62075121); Program for Sanjin Scholars of Shanxi Province; Key Research and Development Program of Shanxi Province for International Cooperation (201803D421034) and the fund for Shanxi '1331 Project'.

References

[1] Ye J 2004 *Opt. Lett.* **29** 1153–5
[2] Lešundák A, Voigt D, Cip O and Berg S 2017 *Opt. Express* **25** 32570–80
[3] Rosenband T *et al* 2008 *Science* **319** 1808–12
[4] Villares G, Hugi A, Blaser S and Faist J 2014 *Nat. Commun.* **5** 5192
[5] Suh M G, Yang Q F, Yang K Y, Yi X and Vahala K J 2016 *Science* **354** 600–3
[6] Porat G, Heyl M C, Schoun B S, Benko C, Dörre N, Corwin L K and Ye J 2018 *Nat. Photon.* **12** 387–91
[7] Solaro C, Meyer S, Fisher K, DePalatis M V and Drewsen M 2018 *Phys. Rev. Lett.* **120** 253601
[8] Wang S D, Yuan J P, Wang L R, Xiao L T and Jia S T 2020 *Front. Phys.* **16** 12502
[9] Liu N, Yuan J P, Wang L R, Xiao L T and Jia S T 2021 *Laser Phys. Lett.* **19** 025201
[10] Cundiff S T and Weiner A M 2010 *Nat. Photon.* **4** 760–6
[11] Shaltout A M, Lagoudakis K G, Groep J, Kim S J, Vučković J, Shalaev V M and Brongersma M L 2019 *Science* **365** 374–7
[12] Terra O 2019 *J. Lightwave Technol.* **37** 5363–9
[13] Liu H, Yin M, Kong D, Xu Q, Zhang S and Chang H 2015 *Appl. Phys. Lett.* **107** 151104
[14] Moon H S, Kim E B, Park S E and Park C Y 2006 *Appl. Phys. Lett.* **89** 181110
[15] Doumbia Y, Wolfersberger D, Panajotov K and Sciamanna M 2021 *Opt. Express* **29** 33976–91
[16] Redding B, McKinney J D, Schermer R T and Murray J B 2022 *Opt. Express* **30** 22097–106
[17] Balakier K, Shams H, Fice M J, Ponnampalam L, Graham C S, Renaud C C and Seeds A J 2018 *J. Lightwave Technol.* **36** 4646–54
[18] Gerhardt I 2018 *Opt. Lett.* **43** 5295–8
[19] Keaveney J, Wrathmall S A, Adams C S and Hughes I G 2018 *Opt. Lett.* **43** 4272–5
[20] Yan Y, Yuan J P, Wang L R, Xiao L T and Jia S T 2022 *Opt. Commun.* **509** 127855
[21] Logue F D, Briscoe J D, Pizzey D, Wrathmall S A and Hughes I G 2022 *Opt. Lett.* **47** 2975–8
[22] Siyushev P, Stein G, Wrachtrup J and Gerhardt I 2014 *Nature* **509** 66–70
[23] Portalupi S L, Widmann M, Nawrath C, Jetter M, Michler P, Wrachtrup J and Gerhardt I 2016 *Nat. Commun.* **7** 13632
[24] Zhuang W and Chen J 2014 *Opt. Lett.* **39** 6339–42
[25] Moon H S, Ryu H Y, Lee S H and Suh H S 2011 *Opt. Express* **19** 15855–63
[26] Yuan J, Wu C, Wang L, Chen G and Jia S 2019 *Opt. Lett.* **44** 4123–6
[27] Yuan J, Zhang H, Wu C, Wang L, Xiao L and Jia S 2021 *Opt. Lett.* **46** 4184–7
[28] Pan T, Chen T, Sun D, Han Y, Xue X, Zhao R and Lan J 2021 *Opt. Express* **29** 4431–41
[29] Zentile M A, Keaveney J, Mathew R S, Whiting D J, Adams C S and Hughes I G 2015 *J. Phys.* B **48** 185001
[30] Higgins C R and Hughes I G 2021 *J. Phys.* B **54** 165403
[31] Stowe M C, Thorpe M J, Pe'er A, Ye J, Stalnaker J E, Gerginov V and Diddams S A 2008 *Adv. At. Mol. Opt. Phys.* **55** 1–60